Global Biogeochemical Cycles®

RESEARCH ARTICLE
10.1029/2021GB007226

Special Section:
Southern Ocean and Climate: Biogeochemical and Physical Fluxes and Processes

Indo-Pacific Sector Dominates Southern Ocean Carbon Outgassing

Channing J. Prend[1], Alison R. Gray[2], Lynne D. Talley[1], Sarah T. Gille[1], F. Alexander Haumann[3,4], Kenneth S. Johnson[5], Stephen C. Riser[2], Isabella Rosso[1], Jade Sauvé[2], and Jorge L. Sarmiento[3]

[1]Scripps Institution of Oceanography, University of California San Diego, La Jolla, CA, USA, [2]School of Oceanography, University of Washington, Seattle, WA, USA, [3]Atmospheric and Oceanic Sciences Program, Princeton University, Princeton, NJ, USA, [4]British Antarctic Survey, Cambridge, UK, [5]Monterey Bay Aquarium Research Institute, Moss Landing, CA, USA

Key Points:

- Autonomous biogeochemical floats reveal that carbon outgassing occurs predominantly in the Indo-Pacific sector of the Southern Ocean
- Asymmetry in carbon outgassing is driven by systematic interbasin variations in the mixed-layer entrainment of carbon-rich deep water
- Expanded data coverage, particularly circumpolar sampling, is necessary to accurately capture Southern Ocean carbon sink variability

Supporting Information:

Supporting Information may be found in the online version of this article.

Correspondence to:

C. J. Prend,
cprend@ucsd.edu

Citation:

Prend, C. J., Gray, A. R., Talley, L. D., Gille, S. T., Haumann, F. A., Johnson, K. S., et al. (2022). Indo-Pacific sector dominates Southern Ocean carbon outgassing. *Global Biogeochemical Cycles*, *36*, e2021GB007226. https://doi.org/10.1029/2021GB007226

Received 12 OCT 2021
Accepted 23 JUN 2022

Abstract The Southern Ocean modulates the climate system by exchanging heat and carbon dioxide (CO_2) between the atmosphere and deep ocean. While this region plays an outsized role in the global oceanic anthropogenic carbon uptake, CO_2 is also released to the atmosphere across large swaths of the Antarctic Circumpolar Current (ACC). Southern Ocean outgassing has long been attributed to remineralized carbon from upwelled deep water, but the precise mechanisms by which this water reaches the surface are not well constrained from observations. Using data from a novel array of autonomous biogeochemical profiling floats, we examine Southern Ocean air-sea CO_2 fluxes and the pathways that transfer carbon from the ocean interior into the mixed layer where air-sea exchange occurs. These float-based flux estimates of unprecedented spatial resolution indicate that carbon outgassing occurs predominantly in the Indo-Pacific sector of the ACC due to variations in the mean surface ocean partial pressure of CO_2 (pCO_2). We show that this zonal asymmetry in surface pCO_2, and consequently air-sea carbon fluxes, stems primarily from regional variability in the mixed-layer entrainment of upwelled carbon-rich deep water. These results suggest that a sustained circumpolar observing system is crucial to monitor future changes in oceanic carbon release and uptake.

Plain Language Summary The Southern Ocean, which surrounds Antarctica, helps regulate the global climate system by sequestering atmospheric heat and carbon dioxide (CO_2) in the deep ocean. Although this region makes a significant contribution to the total oceanic carbon uptake, there are also locations in the Southern Ocean where CO_2 is released back into the atmosphere. Understanding what controls these patterns of air-sea carbon exchange is necessary to improve climate models and prepare for the effects of climate change. However, studying the Southern Ocean carbon cycle is difficult due to the lack of observations from this remote environment. Here, we use new data collected by autonomous biogeochemical floats to examine air-sea carbon fluxes throughout the Southern Ocean. We find that ocean carbon release occurs preferentially in the Indo-Pacific sector of the Southern Ocean due to systematic differences between basins in the transport of subsurface carbon from the deep ocean into the mixed layer—the portion of the upper ocean that is in direct contact with the atmosphere. These results suggest that collecting data from all sectors of the Southern Ocean is crucial to monitor future changes in the ocean carbon sink.

1. Introduction

The Southern Ocean accounts for a disproportionately large percentage of the total oceanic anthropogenic carbon uptake, which results from the region's unique role in the global overturning circulation (Frölicher et al., 2015; Khatiwala et al., 2009). In the southern portion of the Antarctic Circumpolar Current (ACC), deep water returns to the upper ocean via wind-driven upwelling and is transformed into northward-flowing intermediate and bottom waters (J. Marshall & Speer, 2012). These upwelled deep waters have been isolated from the atmosphere since preindustrial times, and thus are poised both to absorb anthropogenic CO_2 and to release natural carbon that has accumulated over centuries through the remineralization of organic matter (Lovenduski et al., 2008). The net air-sea carbon exchange in the Southern Ocean is, therefore, a balance between opposing processes of carbon uptake and outgassing (DeVries et al., 2017; Gruber et al., 2019).

Both uptake of anthropogenic CO_2 and outgassing of natural carbon are fundamentally tied to the physical transport of water between the surface mixed layer and ocean interior. While the circulation of the Southern Ocean has

often been described in a zonally averaged framework (J. Marshall & Speer, 2012), recent work has highlighted significant regional differences in upwelling, mixed-layer dynamics, and their response to climate variability (Rintoul, 2018; Sallée, Speer, & Rintoul, 2010; Tamsitt et al., 2017; Viglione & Thompson, 2016). These zonal variations in the circulation and surface forcing, in turn, impact air-sea heat and carbon exchange (Keppler & Landschützer, 2019; Tamsitt et al., 2015). For example, observation-based estimates and modeling studies suggest that subduction and storage of anthropogenic carbon are highly localized (Bopp et al., 2015; Sallée et al., 2012). Less attention has been paid to the zonal structure of carbon outgassing, in part, because it occurs primarily due to entrainment of subsurface carbon in winter when observations are difficult to obtain (Gray et al., 2018).

Starting in 2014, autonomous biogeochemical profiling floats have been deployed as part of the Southern Ocean Carbon and Climate Observations and Modeling (SOCCOM) project (Talley et al., 2019). The SOCCOM float array was developed to increase the number and distribution of year-round subsurface biogeochemical measurements because of the known importance of the Southern Ocean to the global carbon cycle and the deficiencies of Earth System Models (ESMs) in this region (Beadling et al., 2020; Frölicher et al., 2015; Russell et al., 2018). In situ observations provide an important constraint on climate models, which disagree significantly on the magnitude and variability of Southern Ocean air-sea carbon fluxes (F_{CO_2}) (Anav et al., 2013; Mongwe et al., 2018; Terhaar et al., 2021). Indeed, the net Southern Ocean carbon uptake is a major source of uncertainty in the global carbon budget (Friedlingstein et al., 2020; Le Quéré et al., 2013), and current observation-based estimates rely mainly on sparse surface pCO_2 measurements, which are extended using innovative mapping techniques (Keppler & Landschützer, 2019; Landschützer et al., 2015; Rödenbeck et al., 2013).

Based on the first several years of limited SOCCOM data, Gray et al. (2018) showed a surprisingly large outgassing signal in the southern ACC. Bushinsky et al. (2019) used the growing float record to directly compare SOCCOM-derived fluxes with ship-based fluxes mapped using a neural network (Landschützer et al., 2015) and the Jena CarboScope method (Rödenbeck et al., 2013), as well as the Biogeochemical Southern Ocean State Estimate (B-SOSE) (Verdy & Mazloff, 2017) and an ESM. Bushinsky et al. (2019) similarly showed a higher outgassing in the ACC with the inclusion of SOCCOM float data, in part due to the seasonal bias in ship-based products. These previous analyses have focused on the net Southern Ocean carbon uptake and zonally averaged fluxes, but significant spatial variability in F_{CO_2} has begun to emerge with increasing float coverage. Here, we use data from nearly 200 SOCCOM floats to investigate zonal variations in air-sea carbon exchange as well as the subsurface processes that contribute to these patterns.

We show that carbon outgassing within the ACC occurs preferentially in the Indo-Pacific sector due to a higher annual mean surface ocean pCO_2. This basin asymmetry could potentially result from regional variability in deep water carbon content, mixed-layer entrainment, wind forcing, and/or biological productivity. We assess the relative importance of these mechanisms using the subsurface float data, in combination with several other observational data sets. We find that the interbasin variation in surface ocean pCO_2 is primarily driven by regional variability in wintertime entrainment of carbon-rich deep water from the permanent pycnocline ("obduction"). Namely, we show that zonal asymmetry in the mixed-layer depth (MLD) distribution leads to systematic differences between basins in the fraction of upwelled carbon-rich water that is entrained into the surface mixed layer. Variations in the flux of carbon across the mixed-layer base alone could explain the observed asymmetry in CO_2 outgassing. While MLD is used as a predictor variable in many air-sea carbon flux products (Bushinsky et al., 2019; Rödenbeck et al., 2013), our results provide a direct observational link between the spatial patterns of MLD and F_{CO_2} in the Southern Ocean, which can inform future work investigating model biases.

2. Data and Methods

2.1. Observational Data Sets

This study uses in situ data from autonomous biogeochemical floats deployed by the SOCCOM project. SOCCOM floats measure temperature, salinity, pressure, dissolved oxygen, nitrate, pH, fluorescence, and backscatter over the top 2,000 m of the water column every 10 days (Riser et al., 2018). The quality-controlled data from the 30 August 2020 SOCCOM snapshot are used in this analysis and are publicly available (http://doi.org/10.6075/J0BK19W5). Floats sample unevenly in the vertical, so all profiles are linearly interpolated onto a regular depth axis with 5 m resolution in the upper 500 m, 10 m resolution from 500 to 1,000 m, 50 m resolution from 1,000 to 1,500 m, and 100 m resolution from 1,500 to 2,000 m. The SOCCOM snapshots include estimates of total

alkalinity (TA) from a locally interpolated alkalinity regression (Carter et al., 2017) and pCO_2 calculated from the alkalinity and in situ pH (Williams et al., 2017). We also compute the potential pCO_2 (PCO_2), which is the pCO_2 a water parcel would have if it were raised to the surface adiabatically (Broecker & Peng, 1982; Chen et al., 2022; Skinner et al., 2010), from alkalinity and pH, as well as temperature, salinity, and pressure using the CO_2 System Calculator (CO2SYS) (Humphreys et al., 2020). PCO_2 more directly quantifies the outgassing potential of subsurface waters than other carbon tracers like dissolved inorganic carbon (DIC; discussed further in Section 2.3). For the CO2SYS calculation, we use dissociation constants of carbonate from Lueker et al. (2000), of sulfate from Dickson (1990), and of fluoride from Perez and Fraga (1987), as well as the boron to salinity ratio from Lee et al. (2010).

Additionally, we use data from the full Argo array (Roemmich et al., 2019) up to 30 August 2020, to calculate MLD using a 0.03 kg/m^3 density threshold (Dong et al., 2008). A monthly MLD climatology is developed by mapping all Argo MLD estimates onto a $1° \times 1°$ grid using Gaussian process regression (Kuusela & Stein, 2018). Monthly composites of wind stress from the ERA5 reanalysis product (Hersbach et al., 2020) and absolute geostrophic velocity derived from Argo data (Gray & Riser, 2014) are interpolated onto the same grid to calculate the components of the entrainment rate at monthly resolution (described further in Section 2.3 below). Finally, the mean ACC frontal positions from Kim and Orsi (2014) are used to sort profiles into the Polar Frontal Zone (PFZ) and Antarctic Southern Zone (ASZ). Results are not sensitive to the precise frontal definitions, which were tested by repeating the analysis with fronts determined from the Orsi et al. (1995) temperature and salinity criteria (Gray et al., 2018), and with zones sorted by an unsupervised machine learning classification method (Rosso et al., 2020). We also repeated the analysis using MLD defined by a hybrid algorithm (Holte & Talley, 2009), which did not change the results significantly (not shown).

2.2. Air-Sea Carbon Flux Estimates

Air-sea carbon fluxes are estimated from the profiling float data using the bulk formula (Gray et al., 2018; Wanninkhof, 2014)

$$F_{CO_2} = kK_0 \left(pCO_2^{ocn} - pCO_2^{atm}\right)(1 - SIC), \quad (1)$$

where k is the gas transfer velocity, which is parameterized in terms of the wind speed (Wanninkhof, 2014) and calculated from ERA5 winds collocated with the location and time of each float profile (Hersbach et al., 2020). K_0, the solubility of CO_2 in seawater, depends on temperature and salinity (Weiss, 1974). The surface ocean pCO_2 $\left(pCO_2^{ocn}\right)$ is derived from float pH and empirically estimated alkalinity, as described previously. Measurements of the mole fraction of CO_2 in dry air taken at Cape Grim Observatory (http://www.csiro.au/greenhouse-gases) are utilized to estimate atmospheric pCO_2 $\left(pCO_2^{atm}\right)$ using the sea-level pressure at the float locations from ERA5 and correcting for water vapor pressure (Zeebe & Wolf-Gladrow, 2001). In principle, atmospheric data from Baring Head or South Pole stations could be used to estimate pCO_2^{atm} for the Southern Ocean. However, from 2014 to 2020, the average monthly difference in mole fraction of CO_2 was 0.10 ppm between Cape Grim and Baring Head stations, and 0.25 ppm between Cape Grim and South Pole stations. These differences are small compared to the uncertainty associated with estimating surface ocean pCO_2 from in situ pH, ~11 µatm (Williams et al., 2017). The sea ice concentration (SIC) along each float trajectory is found from daily satellite sea ice extent (Meier et al., 2017). The uncertainty in F_{CO_2} for each float is derived from the uncertainties in each term of Equation 1 using a Monte Carlo simulation. Further details of the air-sea flux calculation and uncertainty estimates are provided in a past study (Gray et al., 2018).

2.3. Obduction Calculation

To assess the mechanisms that transport carbon-rich deep water to the surface ocean, we calculate the obduction fluxes of PCO_2; obduction refers to the mixed-layer entrainment of water from the permanent pycnocline, which was not in contact with the atmosphere during the previous annual cycle. The transfer of fluid into and out of the mixed layer is controlled by changes in the MLD with time, vertical Ekman pumping, and lateral induction (Qiu & Huang, 1995). The instantaneous entrainment rate (E) is the sum of these processes

$$E = \frac{\partial h}{\partial t} + \mathbf{u}_h \cdot \nabla_H h + w_h, \quad (2)$$

where h is the MLD, $\mathbf{u}_h$ and w_h are the lateral and vertical velocities at the base of the mixed layer, respectively, and ∇_H is the horizontal divergence operator (Qiu & Huang, 1995). The terms represent from left to right, the temporal MLD variability, lateral induction associated with horizontal advection of the MLD, and vertical advection. Here, we estimate the entrainment components at monthly resolution using mapped Argo MLD to calculate the temporal and lateral MLD gradients using a central finite difference method. For lateral induction, the horizontal velocity is taken to be the absolute geostrophic velocity (from the Argo-based data product described in Section 2.1) at the depth level closest to the MLD at a given location and month. Vertical velocity is assumed to be dominated by the wind-driven Ekman pumping velocity (Liu & Huang, 2012), which is calculated from monthly composites of ERA5 wind stress.

Given the strong seasonal cycle of MLD, entrainment occurs during the months when the mixed layer deepens. For much of this time, water is entrained from the seasonal pycnocline, which was in contact with the atmosphere in the previous year. The entrainment of water from the permanent pycnocline, which occurs only in late winter near the end of the mixed-layer deepening period, is referred to as obduction (Qiu & Huang, 1995). Water in the permanent pycnocline has been isolated from the atmosphere on long timescales, so obduction is responsible for the transport of upwelled carbon-rich deep water into the mixed layer where it can outgas. The annual mean obduction rate is defined as the instantaneous entrainment rate integrated over the obduction period (Liu & Huang, 2012), taken here to be the 2 months before the maximum winter MLD is reached at a given location (D. Marshall & Marshall, 1995).

To determine the carbon transport associated with each component of obduction, consider the tracer evolution equation integrated over the surface mixed layer,

$$\frac{\partial C_m}{\partial t} = -\mathbf{u}_m \cdot \nabla_H C_m + \kappa_H \nabla_H^2 C_m - \frac{\kappa_z}{h}\frac{\partial C}{\partial z}\bigg|_{z=h} + \left(\frac{C_h - C_m}{h}\right)\left(\frac{\partial h}{\partial t} + \mathbf{u}_h \cdot \nabla_H h + w_h\right) + S_m, \tag{3}$$

where the subscript m represents averaged quantities in the mixed layer, while the subscript h represents the value of a quantity at the mixed-layer base; $\mathbf{u}$ is the horizontal velocity; κ_H and κ_z are the lateral and vertical diffusivities, respectively; and S represents the sources and sinks of carbon such as air-sea fluxes and biological processes. Changes in the mixed-layer carbon content, C_m, are driven by the terms on the right-hand side of the equation. These are from left to right, lateral advection, lateral diffusion, vertical diffusion, entrainment, and the sum of the sources and sinks.

Mixed-layer carbon budgets are typically computed for DIC. However, DIC variability is only one component of surface ocean pCO_2 (Takahashi et al., 2002), which is the quantity relevant to air-sea fluxes. A budget for PCO_2 can be constructed by incorporating terms representing the dependence of surface pCO_2 on temperature, salinity, DIC, and TA. Here, we do not attempt to close a full budget, which is difficult from observations alone. Instead, our goal is to assess the relative size of vertical diffusion and the individual entrainment components, which are the only terms associated with physical transport of fluid from the ocean interior into the mixed layer. Framing the analysis in terms of PCO_2 allows us to directly quantify the impact of obduction on surface pCO_2. However, the calculation was repeated with DIC, which confirmed the conclusions based on PCO_2.

For both PCO_2 and DIC, vertical diffusion is orders of magnitude smaller than entrainment across a range of diffusivities (10^{-4}–10^{-5} m^2/s). While diffusion does not directly drive the changes in mixed-layer pCO_2, it still plays an important role in setting the vertical PCO_2 structure beneath the mixed layer, and hence the carbon content of the waters that are obducted. The annual mean change in mixed-layer pCO_2 due to obduction of subsurface PCO_2 can then be quantified as the product of the entrainment rate integrated over the obduction period and $(C_h - C_m)/h$, or the average PCO_2 difference between the mixed layer and 10 m below the MLD, computed for each float profile and then averaged over the obduction period. This isolates the surface pCO_2 variability due solely to the transfer of high PCO_2 water from the permanent pycnocline into the mixed layer, in other words, the signal related to the outcropping of upwelled deep water. The total uncertainty in the annual mean PCO_2 obduction flux was determined from the uncertainties in each component associated with obduction in Equation 3 using a Monte Carlo simulation with 5,000 iterations for each frontal zone and basin (see Text S1 in Supporting Information S1 for details). We also tested the sensitivity of the results to the assumed length of the obduction period (Text S1 in Supporting Information S1).

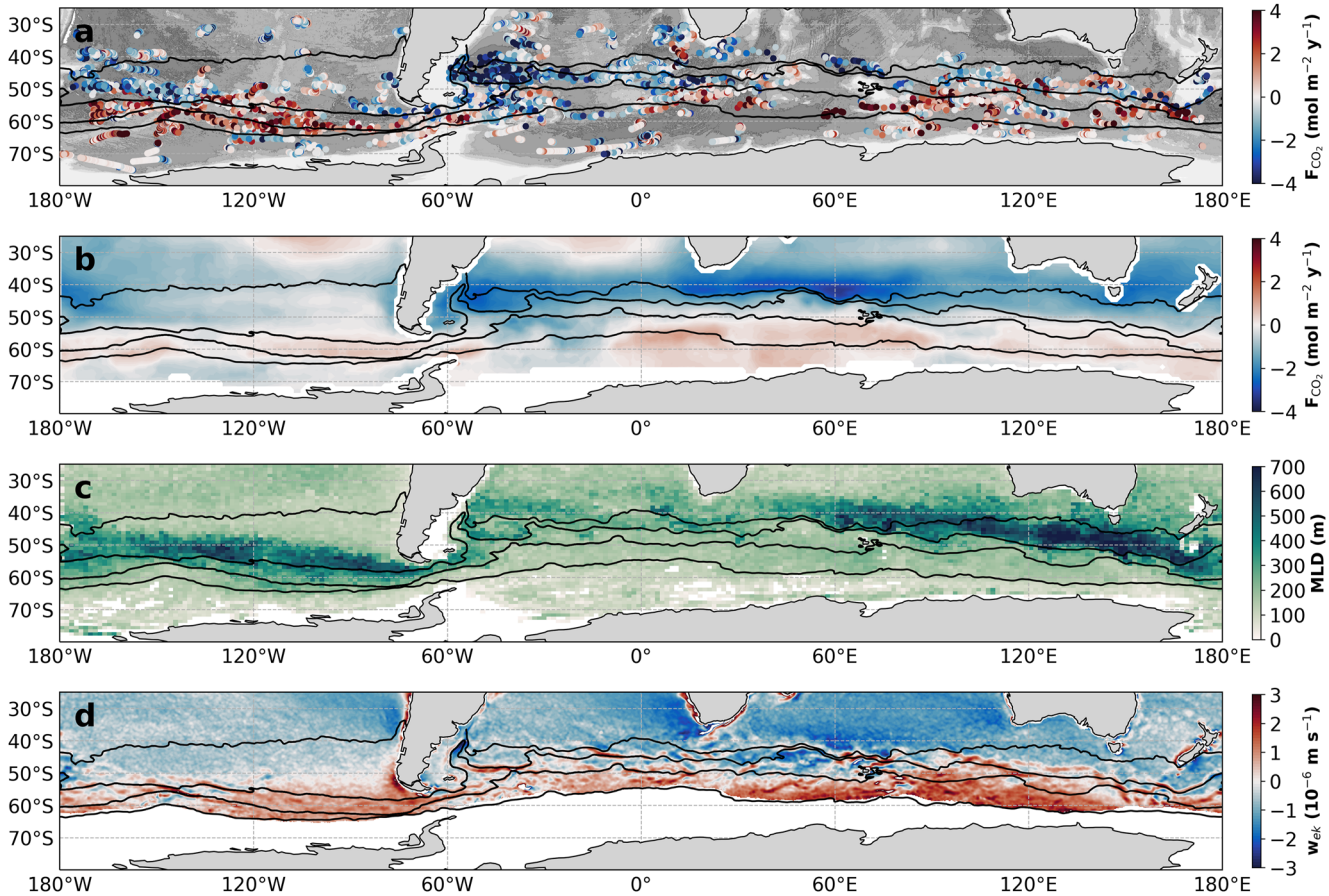

Figure 1. (a) Air-sea CO_2 flux (mol C/m^2/yr) estimated from autonomous biogeochemical float profiles (circles), 2014–2020. Positive flux indicates carbon outgassing from the ocean to the atmosphere. Gray shading marks bathymetry and black lines denote the mean position of the Antarctic Circumpolar Current fronts, which are from north to south: Subtropical front, Subantarctic front, Polar front, and Sea Ice Edge. (b) Annual mean air-sea CO_2 flux (mol C/m^2/yr) from Version 6.6 of the Landschützer climatology, 1982–2021 (Landschützer et al., 2015). (c) Maximum mixed-layer depth (m) in 1° × 1° bins from Argo data, 2000–2020. (d) Annual mean Ekman pumping velocity (10^{-6} m/s) calculated from a scatterometer wind-stress curl climatology (Risien & Chelton, 2008), 1999–2009, where positive velocities denote Ekman upwelling.

3. Results

3.1. Air-Sea Carbon Flux Variability

Float-based air-sea CO_2 flux estimates (Figure 1a) demonstrate significant spatial variability. While carbon outgassing, positive F_{CO_2} in this study, is widespread within the core of the ACC, it is more concentrated in the Indian and Pacific sectors, between Kerguelen Plateau and Drake Passage. This visible asymmetry is unlikely to be due to gaps in float coverage, since it is also visible in the annual mean F_{CO_2} derived from an independent set of pCO_2 measurements from a longer record (Figure 1b) (Landschützer et al., 2015). While the gas transfer velocity can greatly modify the flux magnitude, the sign is set only by the air-sea difference in pCO_2 (Equation 1). Atmospheric CO_2 in the Southern Hemisphere is well-mixed compared to oceanic pCO_2 (Takahashi et al., 1997). Therefore, the distribution of carbon uptake and outgassing is controlled by the surface ocean pCO_2, which in turn varies with temperature, salinity, DIC, and TA (Takahashi et al., 2014).

The components of surface pCO_2 variability exhibit complex spatial patterns, but distinct physical and biogeochemical regimes have been shown to coincide with the ACC frontal zones (Chapman et al., 2020; Gray et al., 2018; Williams et al., 2018). Here, we sort float profiles based on the mean position of the ACC fronts (Kim & Orsi, 2014) (Figure 2a). Throughout the high-latitude Southern Ocean, south of the Subantarctic Front, pCO_2 seasonality is in phase with surface DIC changes (Prend et al., 2022; Takahashi et al., 2014). The seasonal cycle of F_{CO_2}, consequently, shows maximum outgassing in winter when DIC is highest due to respiration and

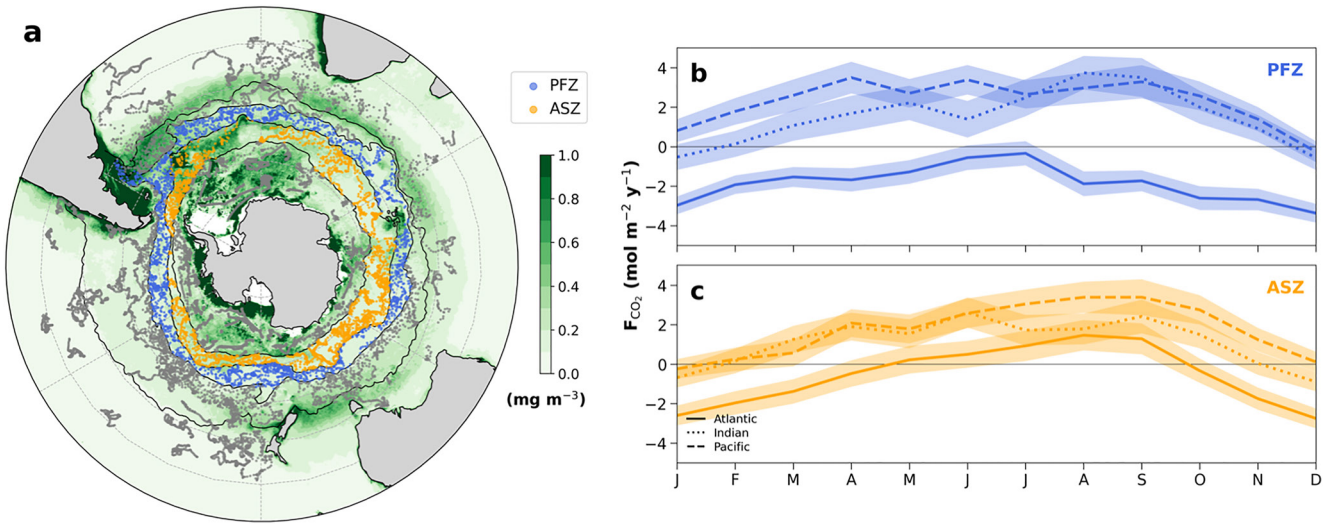

Figure 2. (a) Autonomous biogeochemical float profile locations sorted by frontal zone (PFZ: Polar Frontal Zone; ASZ: Antarctic Southern Zone). Background shading shows austral summer surface chlorophyll (mg/m^3) from a 2002 to 2019 satellite ocean color climatology (NASA Goddard Space Flight Center, Ocean Ecology Laboratory, Ocean Biology Processing Group, 2018). (b) Monthly climatology of air-sea CO_2 flux (mol C/m^2/yr) in the PFZ from float profiles in the Atlantic, 65°W–25°E (solid line), Indian, 25°E–150°E (dotted line), and Pacific, 150°E–65°W (dashed line) sectors. Panel (c) same as panel (b), but for the ASZ.

entrainment of subsurface carbon during deep wintertime mixing (Gray et al., 2018; Williams et al., 2018). Most of the outgassing occurs within the PFZ and ASZ (Gray et al., 2018). However, the fluxes vary strongly with longitude. Monthly climatologies of F_{CO_2} for the PFZ and ASZ indicate significant differences between basins (Figures 2b and 2c; other frontal zones shown in Figure S1 in Supporting Information S1). In the PFZ, outgassing in the Indian and Pacific is compensated by an almost equal magnitude carbon uptake in the Atlantic. Similarly, in the ASZ, outgassing per unit area is significantly higher in the Indo-Pacific compared to the Atlantic.

The variations in F_{CO_2} between basins within the ACC result from large disparities in surface ocean pCO_2 (Figure S2a in Supporting Information S1). The annual mean pCO_2 is higher in the Indo-Pacific than in the Atlantic by 36.7 ± 11.8 µatm in the PFZ and by 17.7 ± 11.1 µatm in the ASZ, where these uncertainties reflect both the variability within each region and the error associated with estimating pCO_2 from in situ pH (Williams et al., 2017). Although the mean pCO_2 differs substantially between basins, particularly in the PFZ, the amplitude of the seasonal cycle, as well as the thermal and nonthermal components of pCO_2 variability, are equivalent across sectors within each frontal zone (Figure S2b in Supporting Information S1). Thus, preferential outgassing in the Indo-Pacific must result from the processes that set the mean surface pCO_2 value, namely, the balance between physical transport of carbon to the mixed layer and biological drawdown (Bronselaer et al., 2018).

Ocean color data demonstrate that patterns of Southern Ocean primary productivity are complex (Figure 2a), and high production in the Atlantic sector likely contributes to the lower pCO_2 values (Arrigo et al., 2008). But while biology can be important locally, its effect is diminished when integrated over an entire basin; at large scales, physical transfers of carbon typically dominate over biological processes (Lévy et al., 2013). Estimates of annual net community production derived from float nitrate drawdown (Johnson et al., 2017; von Berg et al., 2020) (Figure S3 in Supporting Information S1) suggest that export production is higher in the Atlantic by 0.7 ± 1.4 mol C/m^2/yr in the PFZ and 0.4 ± 1.1 mol C/m^2/yr in the ASZ. This difference alone can only account for about 25% of the observed zonal asymmetry of F_{CO_2} within these frontal zones (3.1 and 1.6 mol C/m^2/yr in the PFZ and ASZ, respectively). Therefore, the distribution of mean pCO_2, and thus F_{CO_2}, is most likely primarily related to regional variability in the vertical supply of carbon to the surface ocean.

3.2. Driving Mechanisms

Outgassing in the ACC is associated with Ekman-driven upwelling of carbon-rich deep waters (Lovenduski et al., 2008). However, the transfer of upwelled water into the mixed layer is not as well understood. While past studies have examined surface-to-interior exchange pathways of DIC in models (Lévy et al., 2013), many models

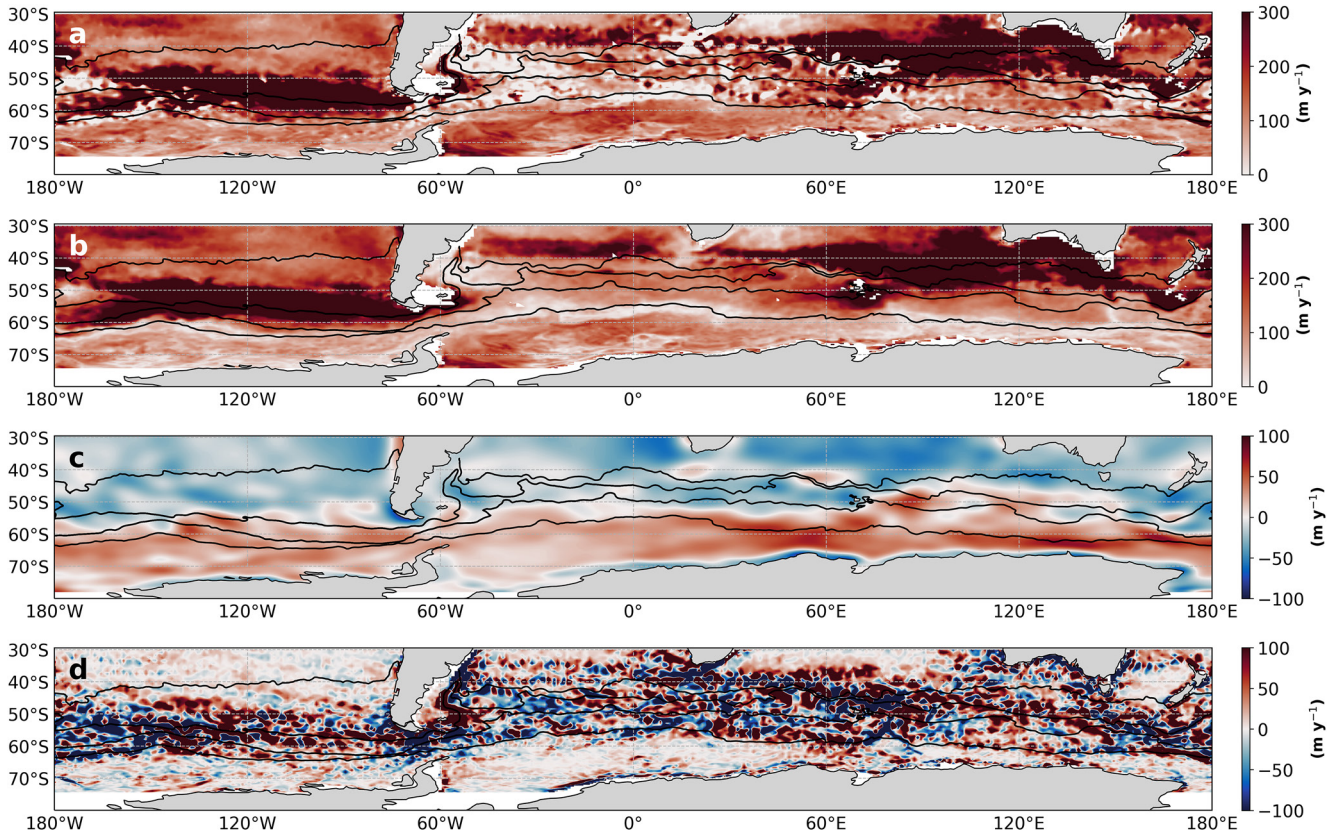

Figure 3. (a) Annual mean obduction rate (m/yr) and contributions due to (b) mixed-layer depth tendency, (c) Ekman pumping velocity, and (d) lateral induction. See Section 2.3 for details of the calculation.

poorly represent the Southern Ocean MLD (Sallée et al., 2013). Consequently, the detailed mechanisms of carbon transport into the Southern Ocean mixed layer are not well constrained, particularly from observations. Recent work has shown that the subsurface PCO_2 maximum coincides with upwelling deep water isopycnal surfaces, providing the source for deep ocean CO_2 release (Chen et al., 2022). To isolate the impact of upwelled deep water on surface pCO_2, we consider the obduction flux of PCO_2, which quantifies the carbon entering the mixed layer from the permanent pycnocline and depends on the obduction rate (Figure 3) as well as the subsurface carbon content. PCO_2 values immediately below the mixed layer (Figures 4d–4f) are largest in the Indian and Pacific sectors due to the comparatively older age of Indo-Pacific Deep Water, which allows for greater accumulation of remineralized carbon (Chen et al., 2022; Heinze et al., 2015; Keppler et al., 2020). This difference in deep water carbon content could contribute to the zonal asymmetry in surface pCO_2 when the water is entrained into the mixed layer. However, within the PFZ and ASZ, the interbasin variation in PCO_2 at the mixed-layer base results primarily from the deeper winter MLDs in the Indo-Pacific, rather than the background PCO_2 profiles (Figures 5b and 5c). Therefore, connectivity between the surface and interior oceans likely varies between basins.

Indeed, there is significant zonal asymmetry in the annual mean obduction rate (Figure 3a), which is dominated by seasonality in the MLD. Therefore, regions of significant obduction (Figure 5a) generally correspond to locations with the deepest maximum MLDs (Figure 1c). Note though that uniform upwelling is needed to continually resupply the subsurface reservoir of carbon-rich deep water. Winter MLDs in the PFZ are roughly 100 m deeper in the Indo-Pacific compared to the Atlantic (Figures 4d–4f). This difference in maximum MLD leads to a larger MLD tendency ($\partial h/\partial t$) and higher PCO_2 at the mixed-layer base during the obduction period in the Indo-Pacific. Both of these induce greater fluxes of PCO_2 into the mixed layer, as the entrainment flux depends on the obduction rate as well as the PCO_2 value of the water being entrained. This is why the strongest outgassing does not correspond to the highest obduction rates and deepest winter mixed layers, which occur in the Subantarctic Zone where carbon-rich isopycnals are too deep to be accessed by wintertime mixing (Figures 4d–4f). It should be noted that high-frequency entrainment events are not captured in this analysis, which uses a monthly

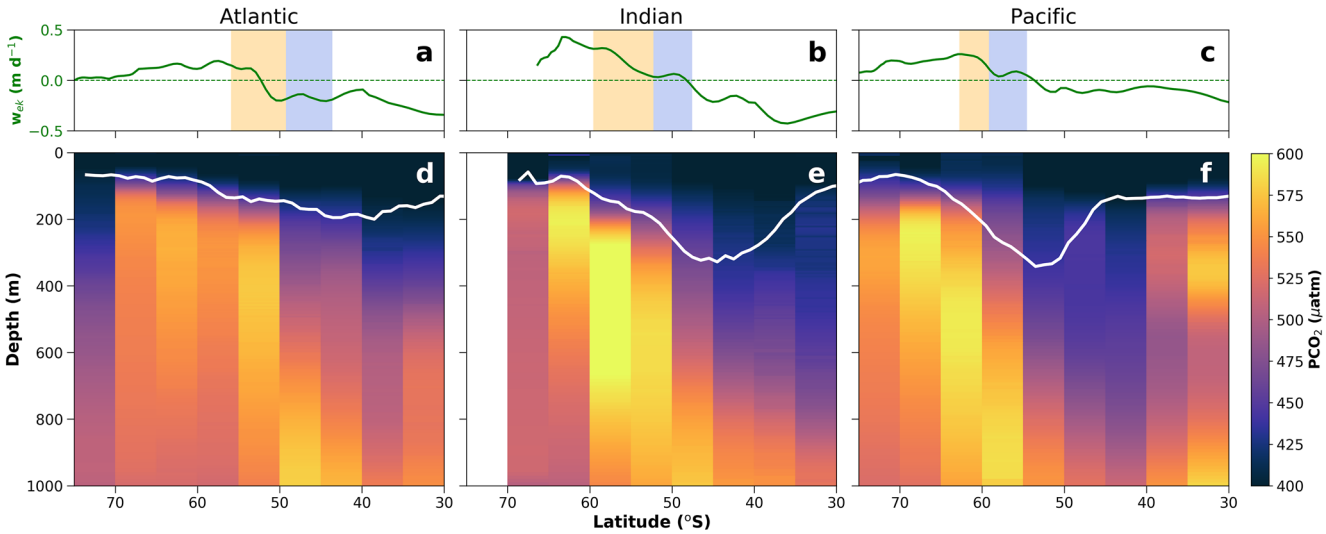

Figure 4. (a–c) Zonally averaged annual mean Ekman pumping velocity (m/d). Shading indicates the mean latitude range of the Polar Frontal Zone (blue) and Antarctic Southern Zone (orange). (d–f) Annual mean PCO_2 (µatm) from autonomous float data zonally averaged in 5° latitude bands with annual maximum mixed-layer depth overlaid in white. Averages are calculated separately for the (a and d) Atlantic, 65°W–25°E, (b and e) Indian, 25°−150°E, and (c and f) Pacific, 150°E−65°W, sectors of the Southern Ocean.

climatology to calculate the temporal MLD variability. Resolving shorter timescales across the entire Southern Ocean, although not possible from the current Argo data coverage, would likely increase the obduction fluxes of carbon in all basins (Freilich & Mahadevan, 2021). However, high-frequency processes, while important locally, may contribute less to the mean basin-scale differences that we focus on here (Lévy et al., 2013; Resplandy et al., 2019).

Ekman pumping accounts for only about 5%–10% of the annual mean obduction rate, but it reinforces the zonal asymmetry in obduction fluxes of carbon (Figures 5d and 5e). Within the PFZ, there are systematic interbasin variations in Ekman pumping resulting from a shift in the mean latitude range of the frontal zones due to topographic steering (Figures 4a–4c). The meridional excursion of the flow downstream of Drake Passage causes ACC streamlines to be furthest north in the Atlantic and to spiral southward across the Indo-Pacific. Therefore, in the PFZ, the mean Ekman pumping velocity (Figure 1d) drives downwelling in the Atlantic and upwelling in the Indian and Pacific. While the Ekman pumping contribution to obduction is small relative to temporal changes in MLD, it plays an important role in setting the PCO_2 value below the MLD. In an abiotic ocean, the vertical PCO_2 structure in the interior results from a balance between the vertical velocity and diffusion (Ito & Follows, 2003). Ekman pumping and diffusion, therefore, increase the proximity of carbon-rich water to the base of the mixed layer, which is necessary for obduction to actually alter the surface pCO_2 value.

The final component of the obduction rate is lateral induction, which is associated with advection across horizontal MLD gradients. This term varies on small scales (Figure 3d). As found in previous studies, lateral induction leads to alternating hotspots of obduction and subduction along the path of the ACC that tend to compensate over large areas (Lévy et al., 2013; Sallée, Speer, Rintoul, & Wijffels, 2010). Because of this compensation effect, the PCO_2 fluxes due to lateral induction are relatively small when averaged over an entire frontal zone and basin (Figures 5d and 5e). While lateral induction can be important on smaller scales and has been suggested to control the locations of anthropogenic carbon subduction (Sallée et al., 2012), its relationship to outgassing is less clear given the long air-sea equilibration timescale for CO_2, which is on the order of 6 months to a year (Jones et al., 2014).

Together, the components of obduction drive an annual change in mixed-layer pCO_2 in the PFZ of approximately 60.6 ± 18.1 µatm in the Indo-Pacific sector and 26.1 ± 13.0 µatm in the Atlantic sector (Figure 5d). The difference between these is roughly equal to the observed difference in annual mean surface pCO_2 between basins in the PFZ (36.7 µatm). In the ASZ, the annual change in mixed-layer pCO_2 due to obduction of subsurface PCO_2 is approximately 44.5 ± 15.7 µatm in the Indo-Pacific and 24.0 ± 14.2 µatm in the Atlantic (Figure 5e).

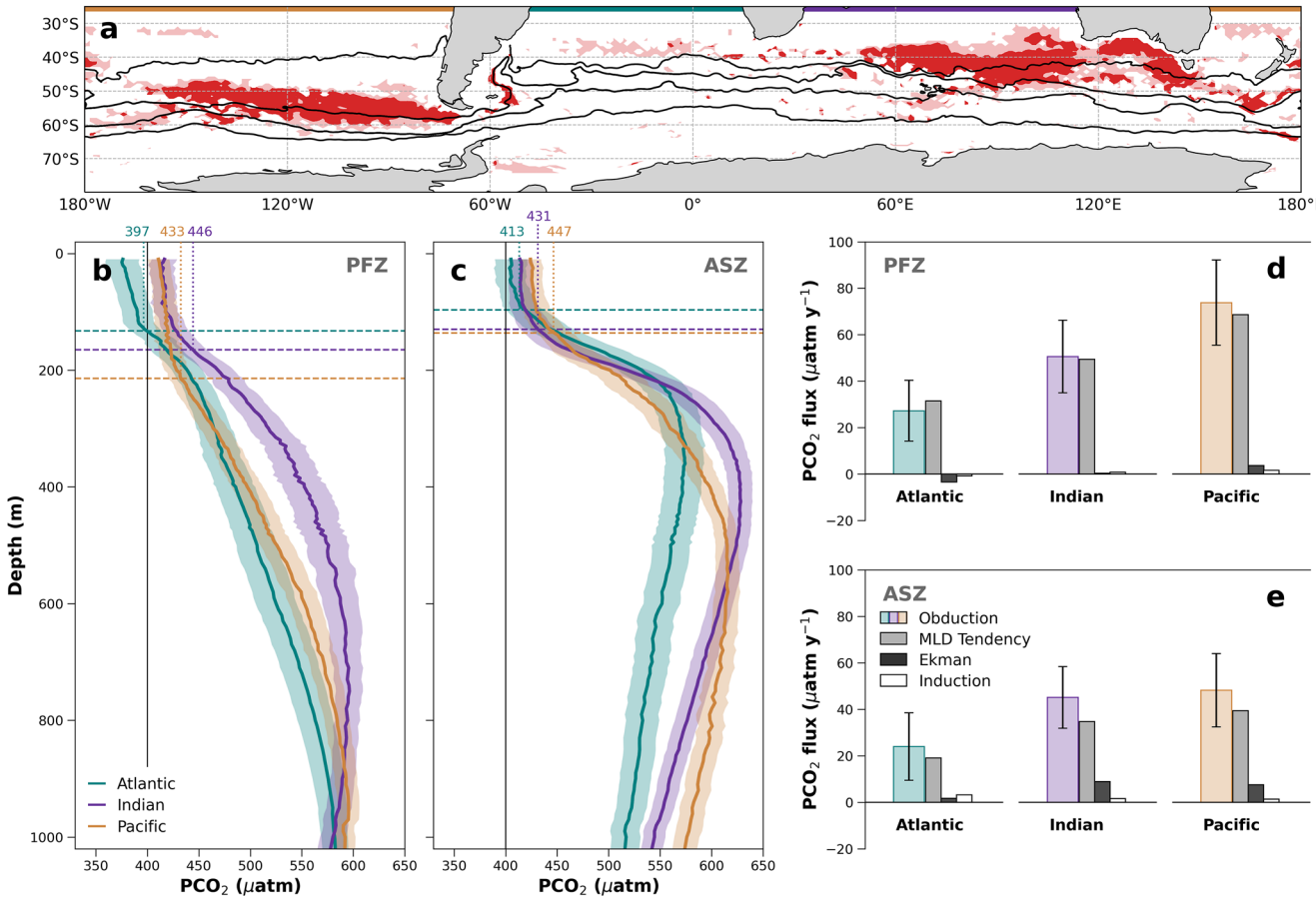

Figure 5. (a) Regions with the largest annual mean obduction rates (200 and 300 m/yr contours plotted in pink and red). (b) Mean vertical profiles of PCO_2 during the obduction period in the Atlantic (teal), Indian (purple), and Pacific (brown) Polar Frontal Zone (PFZ). Horizontal lines mark the mean mixed-layer depth (MLD) in each basin at that time and dotted lines indicate the PCO_2 value at the mean mixed-layer base (values given in raised labels). A black vertical line designates PCO_2 of 400 µatm, the approximate atmospheric value in 2015. (c) Same as (b) for the Antarctic Southern Zone (ASZ). (d) Annual mean PCO_2 obduction fluxes (teal, purple, and brown bars) in the PFZ for each basin, and decomposed into contributions from the MLD tendency (gray), Ekman pumping (black), and lateral induction (white). Panel (e) same as panel (d) for the ASZ.

Again, the difference between the basins is similar to the observed difference in mean surface pCO_2 in the ASZ (17.7 µatm). In other words, the interbasin difference in pCO_2 can be explained almost entirely by regional variability in obduction, although the absolute pCO_2 values will also depend on biological processes and surface heat fluxes. This finding is supported by independent estimates of obduction rates (Liu & Huang, 2012) and Lagrangian mixed-layer outcropping events (Viglione & Thompson, 2016), which show the greatest interior-to-surface exchange in the Pacific sector of the Southern Ocean. Mixed-layer entrainment has been proposed to play a leading role in interannual variability of Southern Ocean carbon fluxes (Verdy et al., 2007), and here we suggest that it is also a key control on the zonal structure of F_{CO_2}.

4. Discussion and Conclusions

High carbon uptake in the temperate latitudes of the Southern Ocean is partially offset by outgassing of remineralized carbon from upwelled deep waters (Anderson et al., 2009). Future changes in the strength of the Southern Ocean carbon sink will depend on the trends in both anthropogenic carbon uptake and natural air-sea carbon exchange (Gruber et al., 2019; Sarmiento et al., 1998), which are not necessarily governed by the same mechanisms (Ito et al., 2010; Lovenduski et al., 2008). Here, we have used novel measurements from autonomous biogeochemical floats to estimate the distribution of Southern Ocean carbon uptake and outgassing. We find persistent differences in the surface ocean pCO_2 and air-sea carbon fluxes between basins within the ACC. The preponderance of outgassing in the Indian and Pacific sectors of the Southern Ocean is linked primarily to zonal

variations in the transport of upwelled deep water into the mixed layer. The obduction fluxes of carbon alone could generate the observed differences in mean surface pCO_2 between basins in both the PFZ and ASZ. These fluxes across the mixed-layer base depend on the obduction rate itself as well as the carbon content of the subsurface waters.

While autonomous floats have significantly increased the spatial and temporal coverage of biogeochemical data in the Southern Ocean, air-sea carbon fluxes exhibit variability across a wide range of scales (Gruber et al., 2019). The magnitude of net air-sea CO_2 exchange across the whole Southern Ocean is likely underconstrained by present-day float data (Bushinsky et al., 2019; Monteiro et al., 2015). Interannual variability is not well resolved either, since the SOCCOM float record only extends back to 2014. However, results do not seem to be influenced by seasonal biases in sampling within a given sector or by having observations heavily skewed toward 1 year in a particular basin (see Text S2, Figures S4 and S5 in Supporting Information S1). Our aim here is not to investigate interannual variability, but rather the drivers of basin-scale differences in mean pCO_2 and F_{CO_2}, which are also seen in observation-based products derived from independent, multidecadal data sets (Landschützer et al., 2015; Takahashi et al., 2002). Understanding these mechanisms provides key context to interpret and predict the response of Southern Ocean carbon fluxes to changes in forcing. Furthermore, as the number of float measurements increases, it will be possible to examine a range of timescales not considered in this analysis.

The interbasin variation of Southern Ocean air-sea carbon fluxes suggests that circumpolar data coverage is necessary to accurately capture the net magnitude and variability of the Southern Ocean carbon sink. For example, temporal fluctuations inferred from upscaled ship-based F_{CO_2} products (Landschützer et al., 2015) may be influenced by the fraction of measurements from each basin in a given year. Furthermore, the heterogeneity of obduction could lead to fundamental differences in how the sectors respond to climate variability. Historical observations from the Southern Ocean are biased to the Atlantic, which has the highest uptake per unit area (Keppler & Landschützer, 2019). Lack of wintertime measurements and limited spatial sampling in the Pacific sector of the ACC could both lead to an underestimation of the overall Southern Ocean carbon outgassing.

Previous observational studies on the Southern Ocean carbon sink have relied primarily on surface pCO_2 measurements (Landschützer et al., 2015) or atmospheric inversions (Le Quéré et al., 2007). While a number of studies have used mixed-layer budgets to investigate air-sea carbon exchange (Bushinsky et al., 2019; Lévy et al., 2013; Rödenbeck et al., 2013; Sallée et al., 2012), the present work is the first to highlight and to mechanistically explain the interbasin differences in Southern Ocean outgassing. Developing this mechanistic understanding requires information about the seasonal cycle and biogeochemical properties in the ocean interior, which is provided by unique year-round and subsurface data from autonomous floats. Our results suggest that obduction plays a leading role in the regional patterns of Southern Ocean air-sea carbon fluxes. However, many ESMs poorly represent the seasonal cycle of Southern Ocean MLD (Sallée et al., 2013), which likely leads to errors in the obduction fluxes of carbon. These inconsistencies in MLD may partly explain the large spread in modeled Southern Ocean carbon sink variability, although biases in F_{CO_2} can result from many factors (Mongwe et al., 2018). Greater knowledge of these processes through increased observations is necessary to improve the representation of the carbon cycle in models and predict the response of the ocean to climate change.

Data Availability Statement

Biogeochemical profiling float data were collected and made freely available by the Southern Ocean Carbon and Climate Observations and Modeling Project (http://soccom.princeton.edu) funded by the National Science Foundation Division of Polar Programs (NSF PLR-1425989), the NASA (NNX14AP49B), and Argo and the NOAA programs that contribute to it. In addition, support for the floats came from the NOAA grant NA20OAR4320271 to the University of Washington. Data from the full Argo array were also used (http://argo.ucsd.edu/), as well as absolute geostrophic velocities derived from Argo data (http://alisonrgray.com/agva/), wind stress and sea-level pressure from the ERA5 reanalysis product (http://doi.org/10.1002/qj.3803), and atmospheric CO_2 from Cape Grim Observatory (http://www.csiro.au/greenhouse-gases).

Acknowledgments
Thanks to Katsumi Matsumoto and an anonymous reviewer for their helpful feedback. Thanks also to Peter Landschützer and Haidi Chen for useful comments. C. J. Prend was supported by a National Science Foundation Graduate Research Fellowship under Grant DGE-1650112. A. R. Gray, L. D. Talley, S. T. Gille, F. A. Haumann, K. S. Johnson, S. C. Riser, I. Rosso, J. Sauvé, and J. L. Sarmiento were supported by the NSF PLR-1425989 and OPP-1936222. A. R. Gray acknowledges additional support through the NSF award OCE-1756882. F. A. Haumann was also supported by the SNSF Grant No. P2EZP2_175162 and P400P2_186681, and the NASA Grant No. 80NSSC19K1115.

References

Anav, A., Friedlingstein, P., Kidston, M., Bopp, L., Ciais, P., Cox, P., et al. (2013). Evaluating the land and ocean components of the global carbon cycle in the CMIP5 Earth System Models. *Journal of Climate*, *26*(18), 6801–6843. https://doi.org/10.1175/jcli-d-12-00417.1

Anderson, R. F., Ali, S., Bradtmiller, L. I., Nielsen, S. H. H., Fleisher, M. Q., Anderson, B. E., & Burckle, L. H. (2009). Wind-driven upwelling in the Southern Ocean and the deglacial rise in atmospheric CO_2. *Science*, *323*(5920), 1443–1448. https://doi.org/10.1126/science.1167441

Arrigo, K. R., van Dijken, G. L., & Bushinsky, S. (2008). Primary production in the Southern Ocean, 1997–2006. *Journal of Geophysical Research*, *113*(C8), C08004. https://doi.org/10.1029/2007jc004551

Beadling, R. L., Russell, J. L., Stouffer, R. J., Mazloff, M., Talley, L. D., Goodman, P. J., et al. (2020). Representation of Southern Ocean properties across coupled model intercomparison project generations: CMIP3 to CMIP6. *Journal of Climate*, *33*(15), 6555–6581. https://doi.org/10.1175/jcli-d-19-0970.1

Bopp, L., Lévy, M., Resplandy, L., & Sallée, J.-B. (2015). Pathways of anthropogenic carbon subduction in the global ocean. *Geophysical Research Letters*, *42*(15), 6416–6423. https://doi.org/10.1002/2015gl065073

Broecker, W. S., & Peng, T.-H. (1982). *Tracers in the sea*. Eldigio Press.

Bronselaer, B., Zanna, L., Munday, D. R., & Lowe, J. (2018). Southern Ocean carbon-wind stress feedback. *Climate Dynamics*, *51*(7–8), 2743–2757. https://doi.org/10.1007/s00382-017-4041-y

Bushinsky, S. M., Landschützer, P., Rödenbeck, C., Gray, A. R., Baker, D., Mazloff, M. R., et al. (2019). Reassessing Southern Ocean air-sea CO_2 flux estimates with the addition of biogeochemical float observations. *Global Biogeochemical Cycles*, *33*(11), 1370–1388. https://doi.org/10.1029/2019gb006176

Carter, B. R., Feely, R. A., Williams, N. L., Dickson, A. G., Fong, M. B., & Takeshita, Y. (2017). Updated methods for global locally interpolated estimation of alkalinity, pH, and nitrate. *Limnology and Oceanography: Methods*, *16*(2), 119–131. https://doi.org/10.1002/lom3.10232

Chapman, C. C., Lea, M.-A., Meyer, A., Sallée, J.-B., & Hindell, M. (2020). Defining Southern Ocean fronts and their influence on biological and physical processes in a changing climate. *Nature Climate Change*, *10*(3), 209–219. https://doi.org/10.1038/s41558-020-0705-4

Chen, H., Haumann, F. A., Talley, L. D., Johnson, K. S., & Sarmiento, J. L. (2022). The deep ocean's carbon exhaust. *Global Biogeochemical Cycles*. https://doi.org/10.1002/essoar.10507757.1

DeVries, T., Holzer, M., & Primeau, F. (2017). Recent increase in oceanic carbon uptake driven by weaker upper-ocean overturning. *Nature*, *542*(7640), 215–218. https://doi.org/10.1038/nature21068

Dickson, A. G. (1990). Standard potential of the reaction: $AgCl(s) + 12H_2(g) = Ag(s) + HCl(aq)$, and the standard acidity constant of the ion HSO_4^- in synthetic sea water from 273.15 to 318.15 K. *The Journal of Chemical Thermodynamics*, *22*(2), 113–127. https://doi.org/10.1016/0021-9614(90)90074-z

Dong, S., Sprintall, J., Gille, S. T., & Talley, L. D. (2008). Southern Ocean mixed-layer depth from Argo float profiles. *Journal of Geophysical Research*, *113*(C6), C06013. https://doi.org/10.1029/2006jc004051

Freilich, M., & Mahadevan, A. (2021). Coherent pathways for subduction from the surface mixed layer at ocean fronts. *Journal of Geophysical Research: Oceans*, *126*(5), e2020JC017042. https://doi.org/10.1029/2020jc017042

Friedlingstein, P., O'Sullivan, M., Jones, M. W., Andrew, R. M., Hauck, O. A., Olsen, A., et al. (2020). Global carbon budget 2020. *Earth System Science Data*, *12*, 3269–3340.

Frölicher, T. L., Sarmiento, J. L., Paynter, D. J., Dunne, J. P., Krasting, J. P., & Winton, M. (2015). Dominance of the Southern Ocean in anthropogenic carbon and heat uptake in CMIP5 models. *Journal of Climate*, *28*(2), 862–886. https://doi.org/10.1175/JCLI-D-14-00117.1

Gray, A. R., Johnson, K. S., Bushinsky, S. M., Riser, S. C., Russell, J. L., Talley, L. D., et al. (2018). Autonomous biogeochemical floats detect significant carbon dioxide outgassing in the high-latitude Southern Ocean. *Geophysical Research Letters*, *45*(17), 9049–9057. https://doi.org/10.1029/2018GL078013

Gray, A. R., & Riser, S. (2014). A global analysis of Sverdrup Balance using absolute geostrophic velocities from Argo. *Journal of Physical Oceanography*, *44*(4), 1213–1229. https://doi.org/10.1175/jpo-d-12-0206.1

Gruber, N., Landschützer, P., & Lovenduski, N. S. (2019). The variable Southern Ocean carbon sink. *Annual Review of Marine Science*, *11*(1), 159–186. https://doi.org/10.1146/annurev-marine-121916-063407

Heinze, C., Meyer, S., Goris, N., Anderson, L., Steinfeldt, R., Chang, N., et al. (2015). The ocean carbon sink: Impacts, vulnerabilities and challenges. *Earth System Dynamics*, *6*(1), 327–358. https://doi.org/10.5194/esd-6-327-2015

Hersbach, H., Bell, B., Berrisford, P., Hirahara, S., Horányi, A., Munoz-Sabater, J., et al. (2020). The ERA5 global reanalysis. *Quaterly Journal of the Royal Meteorological Society*, *146*(730), 1999–2049. https://doi.org/10.1002/qj.3803

Holte, J., & Talley, L. D. (2009). A new algorithm for finding mixed layer depths with applications to Argo data and Subantarctic Mode Water formation. *Journal of Atmospheric and Oceanic Technology*, *26*(9), 1920–1939. https://doi.org/10.1175/2009jtecho543.1

Humphreys, M. P., Gregor, L., Pierrot, D., van Heuven, S. M. A. C., Lewis, E. R., & Wallace, D. W. R. (2020). PyCO2SYS: Marine carbonate system calculations in Python. *Zenodo*. https://doi.org/10.5281/zenodo.3744275

Ito, T., & Follows, M. (2003). Upper ocean control on the solubility pump of CO_2. *Journal of Marine Research*, *61*(4), 465–489. https://doi.org/10.1357/002224003322384898

Ito, T., Woloszyn, M., & Mazloff, M. (2010). Anthropogenic carbon dioxide transport in the Southern Ocean driven by Ekman flow. *Nature*, *463*(7277), 80–83. https://doi.org/10.1038/nature08687

Johnson, K. S., Plant, J. N., Dunne, J. P., Talley, L. D., & Sarmiento, J. L. (2017). Annual nitrate drawdown observed by SOCCOM profiling floats and the relationship to annual net community production. *Journal of Geophysical Research: Oceans*, *122*(8), 6668–6683. https://doi.org/10.1002/2017jc012839

Jones, D. C., Ito, T., Takano, Y., & Hsu, W.-C. (2014). Spatial and seasonal variability of the air-sea equilibration timescale of carbon dioxide. *Global Biogeochemical Cycles*, *28*(11), 1163–1178. https://doi.org/10.1002/2014gb004813

Keppler, L., & Landschützer, P. (2019). Regional wind variability modulates the Southern Ocean carbon sink. *Scientific Reports*, *9*(1), 7384. https://doi.org/10.1038/s41598-019-43826-y

Keppler, L., Landschützer, P., Gruber, N., Lauvset, S. K., & Stemmler, I. (2020). Seasonal carbon dynamics in the near-global ocean. *Global Biogeochemical Cycles*, *34*(12), e2020GB006571. https://doi.org/10.1029/2020gb006571

Khatiwala, S., Primeau, F., & Hall, T. (2009). Reconstruction of the history of anthropogenic CO_2 concentrations in the ocean. *Nature*, *462*(7271), 346–349. https://doi.org/10.1038/nature08526

Kim, Y. S., & Orsi, A. H. (2014). On the variability of Antarctic Circumpolar Current fronts inferred from 1992–2011 altimetry. *Journal of Physical Oceanography*, *44*(12), 3054–3071. https://doi.org/10.1175/jpo-d-13-0217.1

Kuusela, M., & Stein, M. L. (2018). Locally stationary spatio-temporal interpolation of Argo profiling float data. *Proceedings of the Royal Society A*, *474*(2220), 20180400. https://doi.org/10.1098/rspa.2018.0400

Landschützer, P., Gruber, N., Haumann, F. A., Rödenbeck, C., Bakker, D. C. E., van Heuven, S., et al. (2015). The reinvigoration of the Southern Ocean carbon sink. *Science*, *349*(6253), 1221–1224. https://doi.org/10.1126/science.aab2620

Lee, K., Kim, T.-W., Byrne, R. H., Millero, F. J., Feely, R. A., & Liu, Y.-M. (2010). The universal ratio of boron and chlorinity for the North Pacific and North Atlantic oceans. *Geochimica et Cosmochimica Acta*, *74*(6), 1801–1811. https://doi.org/10.1016/j.gca.2009.12.027

Le Quéré, C., Andres, R. J., Boden, T., Conway, T., Houghton, R. A., House, J. I., et al. (2013). The global carbon budget 1959–2011. *Earth System Science Data*, *5*, 165–185.

Le Quéré, C., Rödenbeck, C., Buitenhuis, E. T., Conway, T. J., Langenfelds, R., Gomez, A., et al. (2007). Saturation of the Southern Ocean CO_2 sink due to recent climate change. *Science*, *316*(5832), 1735–1738. https://doi.org/10.1126/science.1136188

Lévy, M., Bopp, L., Karleskind, P., Resplandy, L., Ethe, C., & Pinsard, F. (2013). Physical pathways for carbon transfers between the surface mixed layer and the ocean interior. *Global Biogeochemical Cycles*, *27*(4), 1001–1012. https://doi.org/10.1002/gbc.20092

Liu, L. L., & Huang, R. X. (2012). The global subduction/obduction rates: Their interannual and decadal variability. *Journal of Climate*, *25*(4), 1096–1115. https://doi.org/10.1175/2011jcli4228.1

Lovenduski, N. S., Gruber, N., & Doney, S. C. (2008). Toward a mechanistic understanding of the decadal trends in the Southern Ocean carbon sink. *Global Biogeochemical Cycles*, *22*(3), GB3016. https://doi.org/10.1029/2007GB003139

Lueker, T. J., Dickson, A. G., & Keeling, C. D. (2000). Ocean pCO_2 calculated from dissolved inorganic carbon, alkalinity, and equations for K_1 and K_2: Validation based on laboratory measurements of CO_2 in gas and seawater at equilibrium. *Marine Chemistry*, *70*(1–3), 105–119. https://doi.org/10.1016/s0304-4203(00)00022-0

Marshall, D., & Marshall, J. (1995). On the thermodynamics of subduction. *Journal of Physical Oceanography*, *25*(1), 138–151. https://doi.org/10.1175/1520-0485(1995)025<0138:ottos>2.0.co;2

Marshall, J., & Speer, K. (2012). Closure of the meridional overturning circulation through Southern Ocean upwelling. *Nature Geoscience*, *5*(3), 171–180. https://doi.org/10.1038/ngeo1391

Meier, W. N., Fetterer, F., Savoie, M., Mallory, S., Duerr, R., & Stroeve, J. (2017). *NOAA/NSIDC climate data record of passive microwave sea ice concentration, version 3*. NSIDC: National Snow and Ice Data Center.

Mongwe, N. P., Vichi, M., & Monteiro, P. M. S. (2018). The seasonal cycle of pCO_2 and CO_2 fluxes in the Southern Ocean: Diagnosing anomalies in CMIP5 Earth System Models. *Biogeosciences*, *15*(9), 2851–2872. https://doi.org/10.5194/bg-15-2851-2018

Monteiro, P. M. S., Gregor, L., Lévy, M., Maenner, S., Sabine, C. L., & Swart, S. (2015). Intraseasonal variability linked to sampling alias in air-sea CO_2 fluxes in the Southern Ocean. *Geophysical Research Letters*, *42*(20), 8507–8514. https://doi.org/10.1002/2015gl066009

NASA Goddard Space Flight Center, Ocean Ecology Laboratory, Ocean Biology Processing Group. (2018). Moderate-Resolution Imaging Spectroradiometer (MODIS) aqua chlorophyll data; 2018 Reprocessing. NASA OB.DAAC, Greenbelt, MD, USA. https://doi.org/10.5067/AQUA/MODIS/L3M/CHL/2018

Orsi, A. H., Whitworth, T., & Nowlin, W. D. (1995). On the meridional extent and fronts of the Antarctic Circumpolar Current. *Deep-Sea Research I*, *42*(5), 641–673. https://doi.org/10.1016/0967-0637(95)00021-w

Perez, F. F., & Fraga, F. (1987). Association constant of fluoride and hydrogen ions in seawater. *Marine Chemistry*, *21*(2), 161–168. https://doi.org/10.1016/0304-4203(87)90036-3

Prend, C. J., Hunt, J. M., Mazloff, M. R., Gille, S. T., & Talley, L. D. (2022). Controls on the boundary between thermally and non-thermally driven pCO_2 regimes in the South Pacific. *Geophysical Research Letters*, *49*(9), e2021GL095797. https://doi.org/10.1029/2021gl095797

Qiu, B., & Huang, R. X. (1995). Ventilation of the North Atlantic and North Pacific: Subduction versus obduction. *Journal of Physical Oceanography*, *25*(10), 2374–2390. https://doi.org/10.1175/1520-0485(1995)025<2374:votnaa>2.0.co;2

Resplandy, L., Lévy, M., & McGillicuddy, D. J. (2019). Effects of eddy-driven subduction on ocean biological carbon pump. *Global Biogeochemical Cycles*, *33*(8), 1071–1084. https://doi.org/10.1029/2018gb006125

Rintoul, S. R. (2018). The global influence of localized dynamics in the Southern Ocean. *Nature*, *558*(7709), 209–218. https://doi.org/10.1038/s41586-018-0182-3

Riser, S. C., Swift, D., & Drucker, R. (2018). Profiling floats in SOCCOM: Technical capabilities for studying the Southern Ocean. *Journal of Geophysical Research: Oceans*, *123*(6), 4055–4073. https://doi.org/10.1002/2017jc013419

Risien, C. M., & Chelton, D. B. (2008). A global climatology of surface wind and wind stress fields from eight years of QuikSCAT scatterometer data. *Journal of Physical Oceanography*, *38*(11), 2379–2413. https://doi.org/10.1175/2008jpo3881.1

Rödenbeck, C., Keeling, R. F., Bakker, D. C. E., Metzl, N., Olsen, A., Sabine, C., & Heimann, M. (2013). Global surface-ocean pCO_2 and sea-air CO_2 flux variability from an observation-driven ocean mixed-layer scheme. *Ocean Science*, *9*(2), 193–216. https://doi.org/10.5194/os-9-193-2013

Roemmich, D., Alford, M. H., Claustre, H., Johnson, K., King, B., Moum, J., et al. (2019). On the future of Argo: A global, full-depth, multi-disciplinary array. *Frontiers in Marine Science*, *6*, 439. https://doi.org/10.3389/fmars.2019.00439

Rosso, I., Mazloff, M. R., Talley, L. D., Purkey, S. G., Freeman, N. M., & Maze, G. (2020). Water mass and biogeochemical variability in the Kerguelen sector of the Southern Ocean: A machine learning approach for a mixing hot spot. *Journal of Geophysical Research: Oceans*, *125*(3), e2019JC015877. https://doi.org/10.1029/2019jc015877

Russell, J. L., Kamenkovich, I., Bitz, C., Ferrari, R., Gille, S. T., Goodman, P. J., et al. (2018). Metrics for the evaluation of the Southern Ocean in coupled climate models and Earth System Models. *Journal of Geophysical Research: Oceans*, *123*(5), 3120–3143. https://doi.org/10.1002/2017jc013461

Sallée, J.-B., Matear, R. J., Rintoul, S. R., & Lenton, A. (2012). Localized subduction of anthropogenic carbon dioxide in the Southern Hemisphere oceans. *Nature Geoscience*, *5*(8), 579–584. https://doi.org/10.1038/ngeo1523

Sallée, J.-B., Shuckburgh, E., Bruneau, A., Meijers, A. J. S., Bracegirdle, T. J., & Wang, Z. (2013). Assessment of Southern Ocean mixed-layer depths in CMIP5 models: Historical bias and forcing response. *Journal of Geophysical Research: Oceans*, *118*(4), 1845–1862. https://doi.org/10.1002/jgrc.20157

Sallée, J.-B., Speer, K., Rintoul, S., & Wijffels, S. (2010). Southern Ocean thermocline ventilation. *Journal of Physical Oceanography*, *40*(3), 509–529. https://doi.org/10.1175/2009JPO4291.1

Sallée, J.-B., Speer, K. G., & Rintoul, S. R. (2010). Zonally asymmetric response of the Southern Ocean mixed-layer depth to the Southern Annular Mode. *Nature Geoscience*, *3*(4), 273–279. https://doi.org/10.1038/ngeo812

Sarmiento, J. L., Hughes, T. M. C., Stouffer, R. J., & Manabe, S. (1998). Simulated response of the ocean carbon cycle to anthropogenic climate warming. *Nature*, *393*(6682), 245–249. https://doi.org/10.1038/30455

Skinner, L. C., Fallon, S., Waelbroeck, C., Michel, E., & Barker, S. (2010). Ventilation of the deep Southern Ocean and deglacial CO_2 rise. *Science*, *328*(5982), 1147–1151. https://doi.org/10.1126/science.1183627

Takahashi, T., Feely, R. A., Weiss, R. F., Wanninkhof, R. H., Chipman, D. W., Sutherland, S. C., & Takahashi, T. T. (1997). Global air-sea flux of CO_2: An estimate based on measurements of sea-air pCO_2 difference. *Proceedings of the National Academy of Sciences*, *94*(16), 8292–8299. https://doi.org/10.1073/pnas.94.16.8292

Takahashi, T., Sutherland, S. C., Chipman, D. W., Goddard, J. G., Ho, C., Newberger, T., et al. (2014). Climatological distributions of pH, pCO_2, total CO_2, alkalinity, and $CaCO_3$ saturation in the global surface ocean, and temporal changes at selected locations. *Marine Chemistry*, *164*, 95–125. https://doi.org/10.1016/j.marchem.2014.06.004

Takahashi, T., Sutherland, S. C., Sweeney, C., Poisson, A., Metzl, N., Tilbrook, B., et al. (2002). Global sea-air CO_2 flux based on climatological surface ocean pCO_2, and seasonal biological and temperature effects. *Deep-Sea Research II*, *49*(9–10), 1601–1622. https://doi.org/10.1016/s0967-0645(02)00003-6

Talley, L. D., Rosso, I., Kamenkovich, I., Mazloff, M. R., Wang, J., Boss, E., et al. (2019). Southern Ocean biogeochemical float deployment strategy, with example from the Greenwich Meridian line (GO-SHIP A12). *Journal of Geophysical Research: Oceans*, *124*(1), 403–431. https://doi.org/10.1029/2018jc014059

Tamsitt, V., Drake, H. F., Morrison, A. K., Talley, L. D., Dufour, C. O., Gray, A. R., et al. (2017). Spiraling pathways of global deep waters to the surface of the Southern Ocean. *Nature Communications*, *8*(1), 172. https://doi.org/10.1038/s41467-017-00197-0

Tamsitt, V., Talley, L. D., Mazloff, M. R., & Cerovečki, I. (2015). Zonal variations in the Southern Ocean heat budget. *Journal of Climate*, *29*(18), 6563–6579. https://doi.org/10.1175/jcli-d-15-0630.1

Terhaar, J., Frölicher, T. L., & Joos, F. (2021). Southern Ocean anthropogenic carbon sink constrained by sea surface salinity. *Science Advances*, *7*(18), eabd5964. https://doi.org/10.1126/sciadv.abd5964

Verdy, A., Dutkiewicz, S., Follows, M. J., Marshall, J., & Czaja, A. (2007). Carbon dioxide and oxygen fluxes in the Southern Ocean: Mechanisms of interannual variability. *Global Biogeochemical Cycles*, *21*(2), GB2020. https://doi.org/10.1029/2006gb002916

Verdy, A., & Mazloff, M. R. (2017). A data assimilating model for estimating Southern Ocean biogeochemistry. *Journal of Geophysical Research: Oceans*, *122*(9), 6968–6988. https://doi.org/10.1002/2016jc012650

Viglione, G. A., & Thompson, A. F. (2016). Lagrangian pathways of upwelling in the Southern Ocean. *Journal of Geophysical Research: Oceans*, *121*(8), 6295–6309. https://doi.org/10.1002/2016JC011773

von Berg, L., Prend, C. J., Campbell, E. C., Mazloff, M. R., Talley, L. D., & Gille, S. T. (2020). Weddell Sea phytoplankton blooms modulated by sea ice variability and polynya formation. *Geophysical Research Letters*, *47*(11), e2020GL087954. https://doi.org/10.1029/2020gl087954

Wanninkhof, R. (2014). Relationship between wind speed and gas exchange over the ocean revisited. *Limnology and Oceanography: Methods*, *12*(6), 351–362. https://doi.org/10.4319/lom.2014.12.351

Weiss, R. (1974). Carbon dioxide in water and seawater: The solubility of a non-ideal gas. *Marine Chemistry*, *2*(3), 203–215. https://doi.org/10.1016/0304-4203(74)90015-2

Williams, N. L., Juranek, L. W., Feely, R. A., Johnson, K. S., Sarmiento, J. L., Talley, L. D., et al. (2017). Calculating surface ocean pCO_2 from biogeochemical Argo floats equipped with pH: An uncertainty analysis. *Global Biogeochemical Cycles*, *31*(3), 591–604. https://doi.org/10.1002/2016gb005541

Williams, N. L., Juranek, L. W., Feely, R. A., Russell, J. L., Johnson, K. S., & Hales, B. (2018). Assessment of the carbonate chemistry seasonal cycles in the Southern Ocean from persistent observational platforms. *Journal of Geophysical Research: Oceans*, *123*(7), 4833–4852. https://doi.org/10.1029/2017jc012917

Zeebe, R. E., & Wolf-Gladrow, D. (2001). *CO_2 in seawater: Equilibrium, kinetics, isotopes*. Elsevier.

References From the Supporting Information

Laurindo, L., Mariano, A., & Lumpkin, R. (2017). An improved near-surface velocity climatology for the global ocean from drifter observations. *Deep-Sea Research I*, *124*, 73–92. https://doi.org/10.1016/j.dsr.2017.04.009